IEEE Access
Multidisciplinary | Rapid Review | Open Access Journal

Received November 27, 2020, accepted December 14, 2020, date of publication December 17, 2020,
date of current version December 31, 2020.

Digital Object Identifier 10.1109/ACCESS.2020.3045446

Realization of a Single-Layer Terahertz Magnetic Mirror

QIGEJIAN WANG[1], (Graduate Student Member, IEEE), SHAHRAAM AFSHAR V.[2], HEIKE EBENDORFF-HEIDEPRIEM[3], AND SHAGHIK ATAKARAMIANS[1], (Senior Member, IEEE)

[1]THz Photonics Group, School of Electrical Engineering and Telecommunications, University of New South Wales (UNSW), Sydney, NSW 2052, Australia
[2]Laser Physics and Photonic Devices Laboratories, School of Engineering, University of South Australia (UniSA), Adelaide, SA 5095, Australia
[3]Institute for Photonics and Advanced Sensing and School of Physical Sciences, The University of Adelaide, Adelaide, SA 5005, Australia

Corresponding authors: Qigejian Wang (qigejian.wang@student.unsw.edu.au) and Shaghik Atakaramians (s.atakaramians@unsw.edu.au)

ABSTRACT We experimentally demonstrate a single-layer terahertz dielectric metasurface. The metasurface consists of an array of sub-wavelength fibers. It is shown that this single-layer terahertz metasurface has high transmission window and can also behave like a terahertz magnetic or electric mirror due to the excitation of resonances in the fibers. It is also observed that changing the excitation angle ($\phi > 5°$) leads to appearance of new resonances, which narrows and widens the transmission window for s- and p- polarizations, respectively. By exploring the variation of resonances due to excitation of single, double or array of fibers, we have demonstrated that the individual element resonances can interact and lead to high transmission when the fibers are arranged in an array. The proposed single-layer metasurface that can operate both in transmission and reflection mode, opens new opportunities to develop single-layer terahertz devices for wavefront engineering.

INDEX TERMS Magnetic mirror, metasurface, sub-wavelength fibers, terahertz.

I. INTRODUCTION

Metasurfaces are planar metamaterials, usually composed of periodic, quasi-periodic or random units of sub-wavelength structures [1], [2]. Due to the strong response of each unit structure to the incident light, metasurfaces enable the modification of the amplitude [3]–[6], phase [7]–[10], and polarization [11]–[13] of the local light at sub-wavelength scale. Owing to these characteristics, metasurfaces have been used to develop flat devices such as wave plates [14], flat lenses [9], [15], and wavefront manipulation devices [16]. While sub-wavelength metallic resonant elements have been used as building blocks of metasurfaces [13], [17]–[21], the ohmic loss of metals at higher frequencies limits their applications [22]. As a result, sub-wavelength high index dielectric elements, which also exhibit resonances, have been exploited for developing metasurfaces. The resonances in dielectric elements are due to excitation of Mie-resonance [16], [23]–[25] or Whispering Gallery Mode (WGM) [26]–[30] resonances. In general, the dielectric elements used for metasurface are either three-dimensional [4], [6], [7], [11], [23], [24], [31]–[35] or two-dimensional [9], [16], [25], [36]–[38] elements. Many devices have been designed using the dielectric elements, e.g. reflector and regulator for communication wavelength [31], [36], antenna reflector for microwave [32], magnetic mirror [39] and flat lenses [9]. Two-dimensional metasurfaces with characteristics such as near-unity absorption [40], beam steering with a large diffraction angle [33], [41], and anomalous negative-angle refraction [37] have been demonstrated in optics.

Metasurfaces have been studied for controlling electromagnetic waves in terahertz (THz) spectrum [42], [43]. A number of devices with extraordinary properties have been demonstrated at THz range. Magnetic mirrors have been demonstrated experimentally using THz metasurfaces employing disk-shaped silicon cylinders on a gold substrate [34], silicon cubes on a silica wafer [23], and lithium tantalate rods on metallic substrate [44]. Highly flexible and switchable quarter-wave plates have been realized using copper resonators on a sapphire substrate [45], aluminum wire gratings in polyimide layer [46], and silicon resonators

The associate editor coordinating the review of this manuscript and approving it for publication was Davide Ramaccia.

on metal substrate [47]. THz absorbers (97.5% absorbance at 1.011 THz) based on silicon disks on polymer substrate have also been realized for thermophotovoltaic, imaging, and sensing applications [35]. The majority of these metasurface devices have minimum of two layers, e.g. sub-wavelength disks embedded into a supporting layer such as metal [34] or dielectric insulator [24]. Two-layer devices with metal substrate are highly efficient, but they can only be used in reflection mode. Metasurfaces designed to operate in the transmission mode, have lower overall efficiency due to the existence of supporting layer, usually a low-index dielectric substrate, which introduces losses and decreases the refractive index contrast [35]. Thus, single-layer metasurfaces that can operate both in transmission and reflection modes are highly desired. Recently, a single-layer silicon membrane metasurface has been demonstrated for THz wavefront engineering [38]. However, to the best of our knowledge, a single-layer THz metasurface that can exhibit both electric and magnetic mirror has not been demonstrated experimentally.

Here we develop a novel structure for a single-layer THz metasurface using a periodic array of sub-wavelength fibers. We experimentally demonstrate, for the first time to the best of our knowledge, extraordinary electromagnetic properties of this single-layer structure at THz range; i.e. dielectric electric- or magnetic-mirror characteristics, near-unity transmission or reflection, and wide transmission window due to overlap of resonances. The concept of the structure is based on our previous work, where we demonstrated that Mie or WGM resonances can be excited in a sub-wavelength fiber with a relatively medium refractive index using point source excitation, leading to an enhanced magnetic response in THz frequency range [26]–[28], [48]. It should be noted that in this work we concentrate on frequency range ($0.1-0.6$ THz) where the structure is operating in metasurface [49], [50] and not grating [51], [52] regime. This single-layer metasurface can operate in both reflection and transmission modes, which opens new opportunities to develop single-layer THz devices for wave front engineering.

II. EXPERIMENTAL AND SIMULATION SETUP

Fig. 1(a) illustrates the schematic of the single-layer sub-wavelength fiber array, where R is the radius of the fibers ($R = 125\ \mu$m), and D is the periodicity of the structure ($D = 550\ \mu$m)). The periodicity is chosen to be sub-wavelength (within the limitation of holder fabrication) in order to avoid diffraction grating orders. The fiber diameter is also chosen to be sub-wavelength in order to observe the magnetic and electric dipole (ED)/quadrupole resonances, and consequently magnetic and electric mirror behavior. The fiber pieces are taken from the beginning of a drawing trial prior to achieving equilibrium, thus, the fiber pieces have relatively large radius fluctuation of up to 5 μm. We choose a type of soft glass (F2) as the material of the fiber (circular cross-section), which has refractive index of 2.7 for $f \leq 0.7$ THz and loss tangent value of 0.106 at 0.5 THz [53]. Relatively high refractive index (higher than average refractive index of

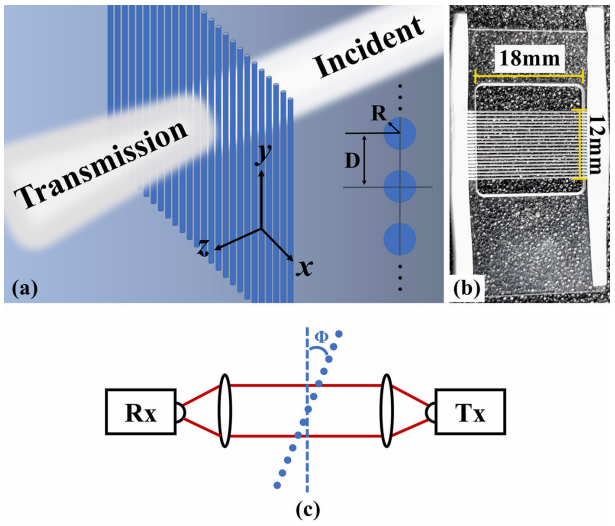

FIGURE 1. (a) Schematic illustration of an incident THz beam on a single-layer array of sub-wavelength fibers. The incident THz wave propagates along z-axis and can be s- or p-polarized. The fibers are made of soft glass (refractive index is $n = 2.7$) with radius $R = 125\ \mu$m, and are arranged in an array with periodicity $D = 550\ \mu$m. (b) Picture of the sample. (c) Schematic illustration of the experimental setup, where Tx is the transmitter and Rx is the receiver.

polymers in THz [35]) is necessary for observation of strong magnetic and electric resonances [28]. Therefore, a soft glass (even though has higher material loss than polymers) is chosen for demonstration of this concept in THz. In order to create the single-layer sample, we use a glass frame, which is grooved with 550 μm of periodicity, and is etched using laser, as shown in Fig. 1(b). The microscope measurement reveals a variation of $511-606\ \mu$m for periodicity and $239-253\ \mu$m for diameter with standard deviations of 25 μm and 4.6 μm, respectively. The array is illuminated by s-polarized (electric field parallel to y axis) and p-polarized (electric field perpendicular to y axis) THz waves.

We use fiber coupled compact THz spectrometer, TeraSmart from Menlo Systems, for measurements, with up to 4.5 THz spectral range and 80 dB dynamic range. The schematic of experimental system is shown in Fig. 1(c). The incident signal on the sample is approximately a Gaussian beam and collimated. The lenses used in this experiment are polymer plano-convex lenses with 50 mm effective focal length. We set an iris with the opening diameter of 10 mm just before the sample to block the stray beams and enable consistent reference and sample measurements.

The results in this work are all normalized transmission, where the measured electric field from the sample is normalized to that of the reference signal. The reference signal is measured when the lenses and iris are in the system without the sample. We rotate the sample to change the incident angle in the experimental setup as shown in Fig. 1(c). There is a gap of 20 mm between the sample and iris, to allow the rotation of the sample to up to 25° for mapping purposes.

We use CST Microwave Studio software to perform the numerical simulation. Unit cell with periodic boundary conditions have been applied to replicate an array of fibers.

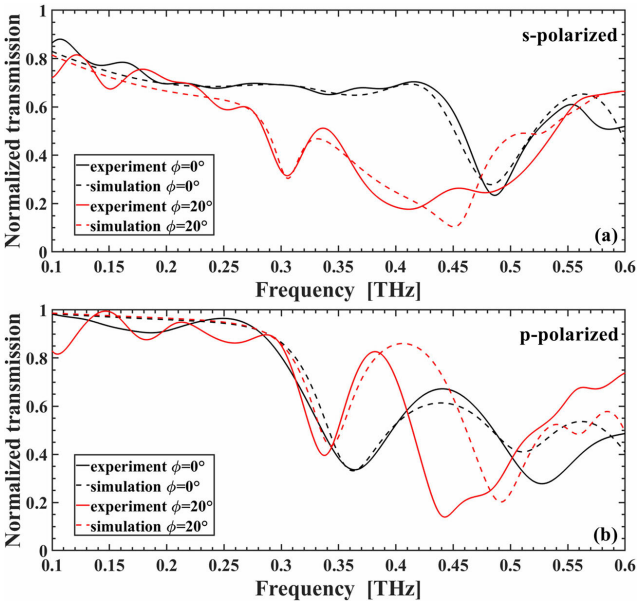

FIGURE 2. Experimental (solid line) and lossy simulated (dash line) normalized electric field amplitude transmission for incident angle of 0 (black line) and 20 degrees (red line) when the sample is illuminated by (a) s-polarized and (b) p-polarized THz beam.

We have used the frequency domain solver with tetrahedral mesh (29436 tetrahedrons per unit cell), and considered a loss tangent value of 0.106 at 0.5 THz for F2 glass material loss in our simulations [53]. The unit cell is excited with a plane wave and the simulation provides the S-parameters, normalized transmitted and reflected electric field, of the periodic lattice. For single/ double/ triple fiber(s) simulations we have defined two ports as transmitter and receiver with the same size as the diameter of the iris we use for measurements.

III. RESULTS AND DISCUSSION

A. ARRAY OF SUB-WAVELENGTH FIBERS

Fig. 2 shows the normalized electric field amplitude transmitted through the fiber-array when the excitation field is s- and p-polarized. We changed the orientation of the emitter and receiver from vertical to horizontal to achieve s- and p-polarization, respectively. Two different incident angles are considered here: ϕ=0° (normal incidence) and ϕ=20°. Overall the experimental measurements match relatively well with the simulation results. We notice that there are oscillations in the experimental results (with average oscillation frequency of 25 GHz), which are due to etalon effect from the lenses (4-mm thick TPX lenses) and diffraction caused by the iris [54]. Similar oscillation has also been observed in [55]. For frequencies less than 0.3 THz, we observe that the transmission for p-polarized waves ($>$ 0.8) is higher than that of the s-polarized waves ($<$ 0.8) when material loss is considered. Whereas, for a lossless array, up to unity transmission (seen later Fig. 3(a) and 4(a)) are observed for both polarizations. For s-polarized wave, the electric field is stronger in the sub-wavelength fibers, which leads to higher losses in the transmission. For p-polarized waves, the electric field is perpendicular to the fibers and more concentrated in the air region. This is due to the fact that normal component of electric field is discontinuous and is enhanced in the air regions between the fibers (Fig. 3(c)), and thus, resulting into a higher transmission compared to that of the s-polarized wave.

For the range of frequencies considered here, 0.1-0.6 THz, the relative periodicity of the array and radius of the fiber to wavelength (D/λ and R/λ) varies from 0.18 to 1.1 and 0.04 to 0.25, respectively. In order to ensure the array operates in the metasurface regime (diffractionless), we need to make sure that the periodicity is smaller than operating wavelength. For this fiber-array sample the incident wavelength equals to the periodicity at $f = 0.55$ THz. Thus, we can state that the array operates at metasurface regime for frequencies less than 0.55 THz.

We observe peaks and dips in the normalized transmission curves, which are due to excitation of resonances (Fig. 2). The excited resonances in the array of fibers can lead to either constructive or destructive interference of the incident THz waves, and the transmission can be enhanced or reduced [16]. The positions of these resonances are different from those of a single fiber, which are observed previously [48]. This is due to the existence of coupling effect between the neighbouring array elements, which leads to shift in the frequency of resonances as well as overlap of resonances (discussed later in III-B) and appearing of new resonances. For normal incidence in Fig. 2, we notice that the frequency of the resonances in experiment and simulation match well when illuminated by s-polarized wave, while there is a slight shift in the resonance frequencies for p-polarized incidence. The dips in transmission, as demonstrated later, indicate that the single-layer dielectric metasurface acts as a reflector. The phase analysis of these resonances (discussed later in this section) reveals that the metasurface behaves like an electric or magnetic mirror at these resonances. We observe emergence of new resonances and changes in the transmission/reflection amplitude by increasing the sample angle. This indicates that there exists resonances that cannot be excited under normal incident (e.g. $f \approx 0.3$ THz for s-polarized excitation). In general, for a resonance to be excited, the symmetry of its field distribution must match that of the excitation, which in this case is achieved when sample is angled. For $\phi = 20°$ excitation, Fig. 2, we observe two dips for both s- and p-polarization. We notice the second dip for both polarizations are slightly shifted between simulation and experiment, where the shift is larger for p-polarized excitation.

A reason for the observed discrepancy (shift) in the frequency of the resonances could be due to the slight variations of periodicity and diameter in the sample. A 20$-\mu$m variation of periodicity shifts the first resonance of p-polarization at normal incidence by 7 GHz. Whereas for 20° incident wave, it shifts 7 GHz and 10 GHz for the first and second s-polarized resonances, respectively, and 5 GHz and 4 GHz for the first and second p-polarized resonances, respectively. A 5 $-\mu$m variation of diameter, for normal incidence, shifts both the

first resonance of s-polarization and the second resonance of p-polarization by 10 GHz. While for 20° incidence, a $5-\mu$m variation of diameter only shifts the s-polarized resonances by 2.5 GHz and p-polarized resonances by 3.75 and 6.25 GHz, respectively. If the fibers are selected from a good draw and in the middle of the fiber then the diameter variations can be less than 1 μm.

Another factor that might contribute more to the observed discrepancies in particular the second dip, is the appearance of the grating lobes (diffraction orders). For the array of fibers with periodicity of D the first grating lobe (first order diffraction) will start appearing for $f > c/(D(1+sin\phi))$, where ϕ is the incident angle. This indicates that the grating lobes will start appearing when $f > 0.54$ and $f > 0.41$ THz for normal ($\phi = 0°$) and oblique ($\phi = 20°$) incidences, respectively. The electric field measured at the receiver end is not the total transmitted field but is rather a portion of the field which is collected by the lens after the sample (see Fig. 1). In our experimental setup, only grating lobes (diffraction orders) with angle less than 20.8°, can be collected and detected (the diameter and focal length of the lens are 38 mm and 50 mm, respectively). Therefore, for $\phi = 25°$ excitation angle (maximum angle measured in the work) we collect and detect only the first grating lobe (first diffraction order) for $f > c/(D(sin\ 20.8° + sin\ 25°)) = 0.7$ THz. As a result, the contributions of higher diffraction orders in the measurement are negligible. While the calculated S-parameters from the simulation are the normalized total transmission and reflection.

To get more insight into the nature of these resonances, we also simulated a lossless array of fibers with the parameters exactly the same as the experimental ones. Fig. 3 (a) and (b) show the simulated p-polarized electric field amplitude and phase of transmitted and reflected THz beam when incident angle is 0°. We have expanded the simulated frequency range to 0.7 THz to include the first three resonances. To have a better understanding, we investigate the electric and magnetic field distributions (Fig. 3 (c)-(f′)) at the position of unity transmission and reflections, which occur due to element or lattice resonances. Around unity transmission ($f = 0.29$ THz), the electric field is stronger on the surface of the fiber due to discontinuity of the field, indicating the lattice coupling can have a great contribution (discussed later in III-B). The remaining resonance points (at $f = 0.36$, 0.51 and 0.64 THz) have unity reflection. The simulated reflected phase of the electric field at $f = 0.36$ and 0.64 THz are close to zero ($2n\pi$), and at $f = 0.51$ THz is π. This indicates that the single-layer metasurface acts as a magnetic mirror (MM) and electric mirror (EM) when the reflected electric phase is zero and π, respectively [56]. Magnetic mirrors form when an array of dominant magnetic dipole (MD) or electric quadrupole (EQ) resonances are oriented as such that the scattered electric fields of these resonances lead to constructive interference in the backward direction [56]. The field distributions at $f = 0.36$ THz (Fig. 3 (d) and (d′)) and $f = 0.64$ THz (Fig. 3 (f) and (f′)) confirm the formation

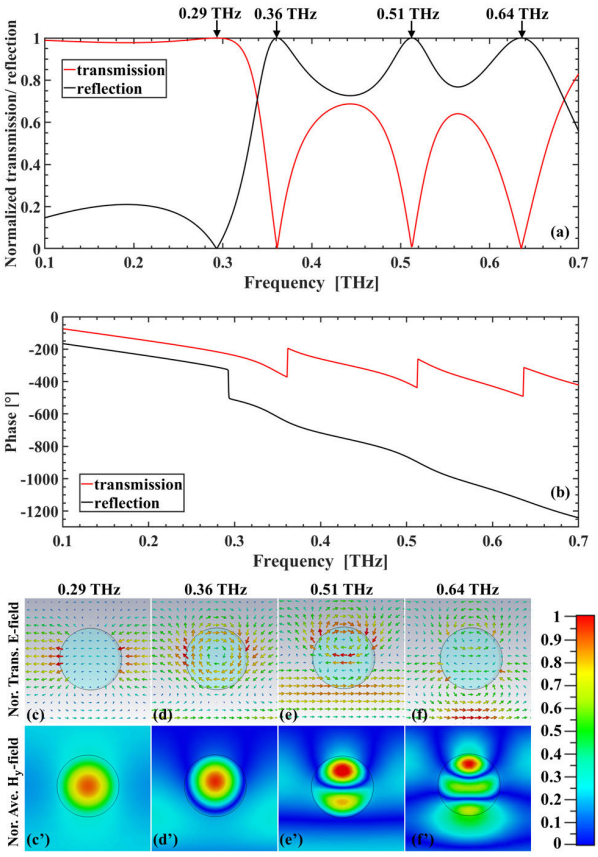

FIGURE 3. Simulated p-polarized electric field (a) amplitude and (b) phase of transmitted (red line) and reflected (black line) THz beam when incident angle is 0°. Normalized transverse average electric field distribution: (c) $f = 0.29$ THz (d) $f = 0.36$ THz (e) $f = 0.51$ THz (f) $f = 0.64$ THz when the curves reach peaks or dips. (c′)-(f′): Corresponding normalized transverse magnetic field distribution of (c)-(f), respectively.

of an array of MD (magnetic field along y-axis and electric field circulating in xz-plane) and EQ in the THz fiber array, respectively. Moreover, Fig. 3 (e) and (e′) also confirm that the structure behaves dominantly as an array of ED at $f = 0.51$ THz, and this is consistent with observation of metasurfaces acting as EM.

Fig. 4 (a) and (b) show the simulated s-polarized electric field amplitude and phase of transmitted and reflected THz beam when incident angle is 0°, respectively. We observe four frequencies in Fig. 4 (a) that have unity transmission or reflection due to the resonances. The first two peaks on transmission curve (red line) are located at $f = 0.34$ and 0.41 THz. The corresponding field distributions indicate that there exists a dominant contribution of MD resonance along x-axis (magnetic field along x-axis and electric field circulating in yz-plane) and ED resonance along y-axis between the fibers (electric field along y-axis and magnetic field circulating in xy-plane), respectively, which leads to unity transmission. Unlike p-polarization, the orientation of the dipole arrays for s-polarization leads to constructive interference in the forward and destructive in the backward direction. The reflection peak is located at $f = 0.48$ THz.

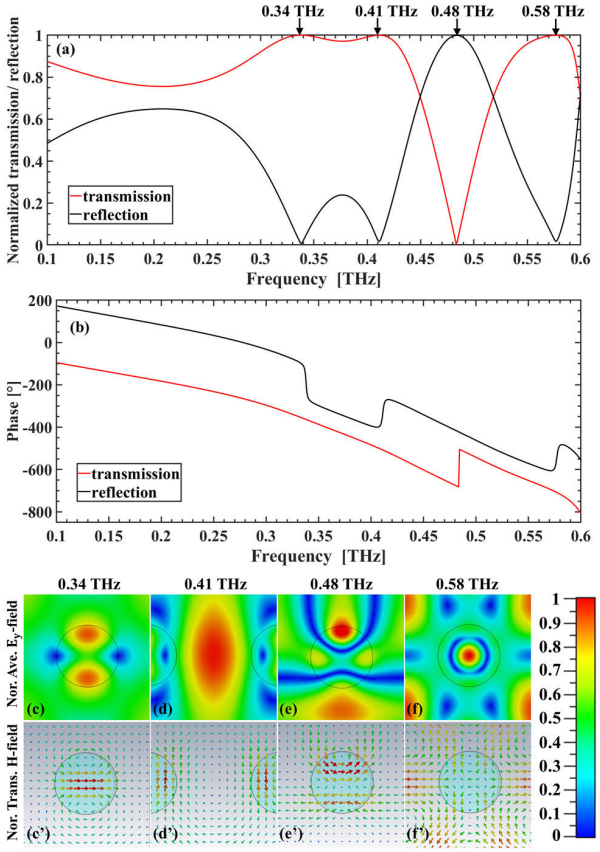

FIGURE 4. Simulated s-polarized electric field (a) amplitude and (b) phase of transmitted (red line) and reflected (black line) THz beam when incident angle is 0°. Normalized transverse average electric field distribution: (c) $f = 0.34$ THz (d) $f = 0.41$ THz (e) $f = 0.48$ THz (f) $f = 0.58$ THz when the curves reach peaks or dips. (c′)-(f′): Corresponding normalized transverse magnetic field distribution of (c)-(f), respectively.

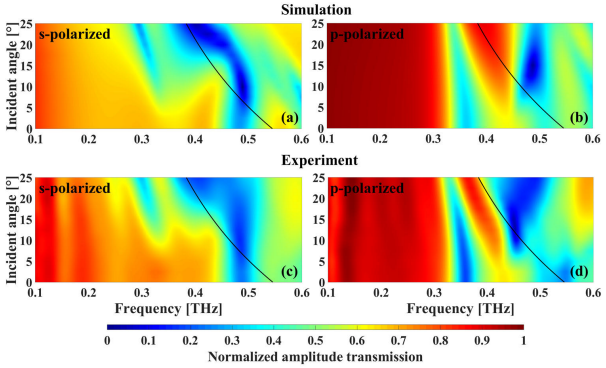

FIGURE 5. The normalized transmitted electric field amplitude as a function of frequency with incident angle from 0° to 25°. Black lines are where the first diffraction order appears. (a) and (c): Lossy simulation and experimental results for s-polarized incident waves, respectively. (b) and (d): Lossy simulated and experimental results for p-polarized incident waves, respectively.

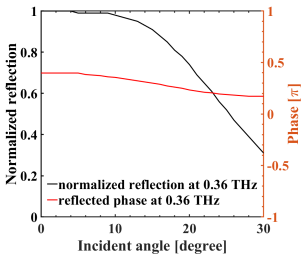

FIGURE 6. Angular dependence of normalized reflection and phase for the magnetic mirror point at 0.36 THz for p-polarization.

The field distributions (Fig. 4 (e) and (e′)) indicate formation of a dominant quadrupole. The multipole decomposition of a silicon array of cylinders indicates that for s-polarized excitation there exists contribution of ED, MD, and magnetic quadrupole (MQ) resonances around similar normalized frequencies [56]. Simulated reflected phase of the electric field at this position is around $-62°$. We attribute this deviation of the phase to the existence of multipolar resonance component. As shown in [56], there exists a mixed excitation of resonances (MD, ED and MQ) at such normalized diameters. This is while, as also stated in Ref. [56], an array of ED/MQ with π reflected phase can lead to EM, and an array of MD/EQ with zero reflected phase can lead to MM. This indicates if the contribution of other resonances (in this case ED and MQ) are strong then the phase of the reflected signal will deviate from π. The third peak of transmission is at 0.58 THz. The corresponding field distributions indicate there exists a strong lattice interaction between the array elements, leading to constructive interference in the forward direction.

For THz wireless telecommunication, beam steering is highly desired to give directionality and increase efficiency, especially at low power transmission. Therefore, we have studied the effect of incident angle on the performance of the metasurface. Fig. 5 shows the normalized simulated and experimentally measured transmitted amplitude of electric field as functions of frequency and incident angle (ϕ) for both polarizations. There is a good agreement between simulations (Fig. 5(a) and (b)) and measurements (Fig. 5(c) and (d)) for $0.1 < f < 0.6$ THz and $0° < \phi < 25°$. The black lines represent the limit beyond which the fiber array will not be operating at metasurface regime and where the first order diffraction kicks in, and cannot be measured in the experiments. This leads to slight difference on the right side of the black lines between simulated and experimental results, especially for p-polarization. As ϕ increases, for s-polarized incident wave (Fig. 5(a) and (c)), the low amplitude transmission (blue range) around 0.5 THz becomes wider and shifts to lower frequencies. We also observe appearance of new resonances around 0.33 THz for $\phi > 5°$, which reduces the high transmission window. While for p-polarized incidence shown in Fig. 5(b) and (d), the low amplitude transmission (blue range) around 0.35 THz becomes narrower as the incident angle increases, which means large incident angle weakens the magnetic mirror effect at this frequency (Fig. 6). A second high transmission window appears around 0.4 THz, which becomes wider as incident angle increases, leading into a wider high transmission window for p-polarized incidence.

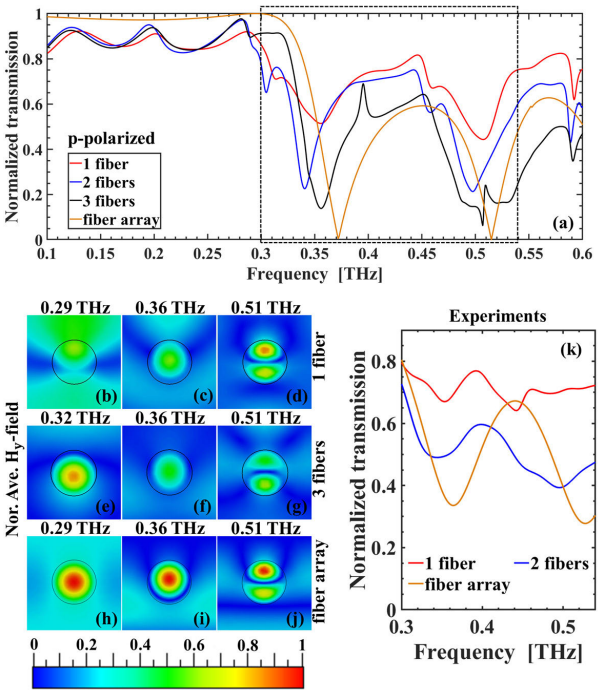

FIGURE 7. (a): Simulated p-polarized electric field amplitude of transmitted THz beam for 1, 2, 3, and infinite fibers when incident angle is 0. Dash-line box indicates the experimental frequency range showed in (k). (b-j): Normalized transverse average magnetic field distribution of single fiber, the middle one of a three-fiber array, and the unit cell of a infinite array. (k): Experimental p-polarized normalized electric field amplitude transmission for 1, 2, and infinite fibers when incident angle is 0.

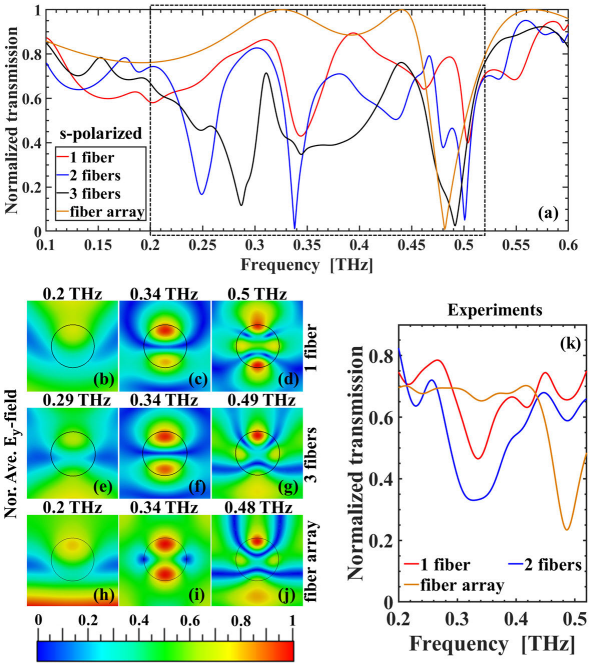

FIGURE 8. (a): Simulated s-polarized electric field amplitude of transmitted THz beam for 1, 2, 3, and infinite fibers when incident angle is 0. Dash-line box indicates the experimental frequency range showed in (k). (b-j): Normalized transverse average electric field distribution of single fiber, the middle one of a three-fiber array, and the unit cell of a infinite array. (k): Experimental s-polarized normalized electric field amplitude transmission for 1, 2, and infinite fibers when incident angle is 0.

B. INDIVIDUAL AND COLLECTIVE RESONANCES: FROM ONE FIBER TO AN ARRAY OF FIBERS

To have a better understanding of the coupling effect between neighboring elements in the array and individual resonances in the elements, here we investigate the transmission characteristics of one, two, three fibers, and compare the results to that of fiber array. The theory of multipolar resonance for an individual rod has been elaborated carefully in [28], [56]. For p-polarization, the transmission (Fig. 7 (a)) enhances and gets close to unity for the array for $0.1 - 0.3$ THz frequency range compared to that of 1, 2, and 3 fiber(s). As stated earlier this is due to enhancement of electric field in sub-wavelength regions in between the fibers, and also confirms the effect of near-field interaction between the lattice element plays a significant role in the unity transmission. We also observe the two resonances (around 0.36 and 0.51 THz) exist regardless whether it is a single fiber or an array. Adding number of elements shifts the resonance position and diminishes the transmission, leading to zero transmission at $f = 0.36$ and $f = 0.51$ THz for lossless infinite fiber array. This also can be verified by experiments (Fig. 7 (k)), where the position of the dips shifts and transmission decreases. This indicates that the collective effect of individual element resonances (near-field interaction) in dielectric array can lead to constructive and destructive interference. The normalized y-component of magnetic field of the single fiber, three fibers, and the fiber array at the position of the dips (Fig. 7 (b)-(j)) confirm that the dips are the same nature of the resonance.

For s-polarization, the high transmission window widens at lower frequency as we increase the number of fibers (Fig. 8 (a)). The weak resonance dips at 0.2 and 0.34 THz for single fiber are shifted towards each other as we increase the number of fibers. It is observed that the first dip shifts faster to higher frequency and eventually overlaps with the second dip, resulting in high transmission. Similar to p-polarization, increasing the number of fibers diminishes the transmission and slightly shifts the third resonance to lower frequencies, and it eventually becomes zero transmission at 0.48 THz for fiber array. The above mentioned points are also observed in the experiments (Fig. 7 (k)), where the dips at 0.22 and 0.34 THz disappear and become flat transmission curve for fiber array. The dip at 0.5 THz shifts and the transmission decreases. The normalized y-component of the electric field of single fiber, three fibers, and the fiber array (Fig. 8(b)-(j)) confirm that the nature of the resonances at the position of the dips for all three scenarios and unity-transmission point for fiber array are the same.

In summary, we observe that coupling effect due to neighboring elements in the fiber array can diminish the transmission (resulting close to unity reflection) or can lead to unity transmission due to resonances overlap.

IV. CONCLUSION AND OUTLOOK

We have experimentally and numerically demonstrated that a single layer of sub-wavelength fibers can display extraordinary electromagnetic proprieties in THz range due to the excitation of resonances in fiber and the lattice coupling. Without the material loss, such an array exhibits unity transmission and reflection at the position of these resonances. We have demonstrated that the array can act as a single-layer all dielectric THz magnetic mirror. We have also demonstrated that a wide transmission window for s-polarized excitation is achieved due to the overlap of resonances in the array. Introducing the loss reduces the transmission peaks from unity to around 70% and 90% for s- and p-polarized excitation, respectively. We also observed appearance of resonances under oblique incidence ($\phi > 5°$), leading to narrower and wider transmission window for s- and p-polarized excitation respectively.

It is expected that using materials with lower material loss at THz (e.g. high-resistivity silicon), instead of F2 soft glass will improve the quality of the magnetic mirror (close to unity transmission and reflection peaks). It should be noted that in this case for silicon, the diameter of the fibers needs to be scaled down to order of $100 - 150$ μm, due to higher refractive index of silicon (3.6) [57]. Fabrication of silicon fiber with such diameters is difficult with the existing fiber drawing technology.

The proposed single-layer THz metasurface paves the path to develop single-layer THz devices for wavefront engineering. Using fibers with different diameters can be considered within a period (hybrid period), which may potentially lead to appearance of more resonances, providing more flexibility in designing THz metadevices.

ACKNOWLEDGMENT

The authors thank Prof Heike Ebendorff-Heidepriem from University of Adelaide for discussion on F2 fiber samples. The microscope image of the sample was taken at the UNSW Node of the Australian National Fabrication Facility.

REFERENCES

[1] C. L. Holloway, E. F. Kuester, J. A. Gordon, J. O'Hara, J. Booth, and D. R. Smith, "An overview of the theory and applications of metasurfaces: The two-dimensional equivalents of metamaterials," *IEEE Antennas Propag. Mag.*, vol. 54, no. 2, pp. 10–35, Apr. 2012.

[2] A. V. Kildishev, A. Boltasseva, and V. M. Shalaev, "Planar photonics with metasurfaces," *Science*, vol. 339, no. 6125, 2013, Art. no. 1232009.

[3] N. M. Estakhri and A. Alá, "Recent progress in gradient metasurfaces," *J. Opt. Soc. Amer. B, Opt. Phys.*, vol. 33, no. 2, p. A21, 2016.

[4] I. Staude, A. E. Miroshnichenko, M. Decker, N. T. Fofang, S. Liu, E. Gonzales, J. Dominguez, T. S. Luk, D. N. Neshev, I. Brener, and Y. Kivshar, "Tailoring directional scattering through magnetic and electric resonances in subwavelength silicon nanodisks," *ACS Nano*, vol. 7, no. 9, pp. 7824–7832, Sep. 2013.

[5] L. Liu, X. Zhang, M. Kenney, X. Su, N. Xu, C. Ouyang, Y. Shi, J. Han, W. Zhang, and S. Zhang, "Broadband metasurfaces with simultaneous control of phase and amplitude," *Adv. Mater.*, vol. 26, no. 29, pp. 5031–5036, Aug. 2014.

[6] S. Liu, M. B. Sinclair, T. S. Mahony, Y. C. Jun, S. Campione, J. Ginn, D. A. Bender, J. R. Wendt, J. F. Ihlefeld, P. G. Clem, J. B. Wright, and I. Brener, "Optical magnetic mirrors without metals," *Optica*, vol. 1, no. 4, pp. 250–256, 2014.

[7] D. Lin, P. Fan, E. Hasman, and M. L. Brongersma, "Dielectric gradient metasurface optical elements," *Science*, vol. 345, no. 6194, pp. 298–302, 2014.

[8] X. Zhang, Z. Tian, W. Yue, J. Gu, S. Zhang, J. Han, and W. Zhang, "Broadband terahertz wave deflection based on C-shape complex metamaterials with phase discontinuities," *Adv. Mater.*, vol. 25, no. 33, pp. 4567–4572, Sep. 2013.

[9] F. Aieta, M. A. Kats, P. Genevet, and F. Capasso, "Multiwavelength achromatic metasurfaces by dispersive phase compensation," *Science*, vol. 347, no. 6228, pp. 1342–1345, Mar. 2015.

[10] N. Yu, P. Genevet, M. A. Kats, F. Aieta, J.-P. Tetienne, F. Capasso, and Z. Gaburro, "Light propagation with phase discontinuities: Generalized laws of reflection and refraction," *Science*, vol. 334, no. 6054, pp. 333–337, Oct. 2011.

[11] Y. Yang, W. Wang, P. Moitra, I. I. Kravchenko, D. P. Briggs, and J. Valentine, "Dielectric meta-reflectarray for broadband linear polarization conversion and optical vortex generation," *Nano Lett.*, vol. 14, no. 3, pp. 1394–1399, Mar. 2014.

[12] W. S. L. Lee, C. Fumeaux, and W. Withayachumnankul, "Metasurfaces for terahertz polarimetry," in *Proc. IEEE Asia–Pacific Conf. Antennas Propag. (APCAP)*, Aug. 2018, pp. 514–516.

[13] T. Ellenbogen, K. Seo, and K. B. Crozier, "Chromatic plasmonic polarizers for active visible color filtering and polarimetry," *Nano Lett.*, vol. 12, no. 2, pp. 1026–1031, Feb. 2012.

[14] E. O. Owiti, H. Yang, C. F. Ominde, and X. Sun, "Broadband quarter-wave plate based on dielectric-embedded plasmonic metasurface," *RSC Adv.*, vol. 7, no. 60, pp. 37495–37501, 2017.

[15] F. Aieta, P. Genevet, M. A. Kats, N. Yu, R. Blanchard, Z. Gaburro, and F. Capasso, "Aberration-free ultrathin flat lenses and axicons at telecom wavelengths based on plasmonic metasurfaces," *Nano Lett.*, vol. 12, no. 9, pp. 4932–4936, Sep. 2012.

[16] W. Liu and A. E. Miroshnichenko, "Beam steering with dielectric metalattices," *ACS Photon.*, vol. 5, no. 5, pp. 1733–1741, May 2018.

[17] J. Linnet, A. R. Walther, C. Wolff, O. Albrektsen, N. A. Mortensen, and J. Kjelstrup-Hansen, "Transparent and conductive electrodes by large-scale nano-structuring of noble metal thin-films," *Opt. Mater. Exp.*, vol. 8, no. 7, pp. 1733–1746, 2018.

[18] M. Tanaka, F. Miyamaru, M. Hangyo, T. Tanaka, M. Akazawa, and E. Sano, "Effect of a thin dielectric layer on terahertz transmission characteristics for metal hole arrays," *Opt. Lett.*, vol. 30, no. 10, pp. 1210–1212, May 2005.

[19] H. Cao and A. Nahata, "Resonantly enhanced transmission of terahertz radiation through a periodic array of subwavelength apertures," *Opt. Exp.*, vol. 12, no. 6, pp. 1004–1010, Apr. 2004.

[20] D. Qu, D. Grischkowsky, and W. Zhang, "Terahertz transmission properties of thin, subwavelength metallic hole arrays," *Opt. Lett.*, vol. 29, no. 8, pp. 896–898, 2004.

[21] T. J. Yen, "Terahertz magnetic response from artificial materials," *Science*, vol. 303, no. 5663, pp. 1494–1496, Mar. 2004.

[22] K. Wang and D. M. Mittleman, "Metal wires for terahertz wave guiding," *Nature*, vol. 432, no. 7015, p. 376, 2004.

[23] Z. Ma, S. M. Hanham, P. Albella, B. Ng, H. T. Lu, Y. Gong, S. A. Maier, and M. Hong, "Terahertz all-dielectric magnetic mirror metasurfaces," *Acs Photon.*, vol. 3, no. 6, pp. 1010–1018, 2016.

[24] J. Tian, Y. Yang, M. Qiu, F. Laurell, V. Pasiskevicius, and H. Jang, "All-dielectric ktiopo 4 metasurfaces based on multipolar resonances in the terahertz region," *Opt. Exp.*, vol. 25, no. 20, pp. 24068–24080, 2017.

[25] P. Spinelli, M. A. Verschuuren, and A. Polman, "Broadband omnidirectional antireflection coating based on subwavelength surface mie resonators," *Nature Commun.*, vol. 3, no. 1, p. 692, Jan. 2012.

[26] S. Atakaramians, F. Q. Dong, T. M. Monro, and S. Afshar V., "Radiated and guided optical waves of a magnetic dipole-nanofiber system," *Sci. Rep.*, vol. 9, no. 1, Mar. 2019, Art. no. 3568.

[27] S. Afshar V, M. R. Henderson, A. D. Greentree, B. C. Gibson, and T. M. Monro, "Self-formed cavity quantum electrodynamics in coupled dipole cylindrical-waveguide systems," *Opt. Exp.*, vol. 22, no. 9, pp. 11301–11311, 2014.

[28] S. Atakaramians, A. E. Miroshnichenko, I. V. Shadrivov, A. Mirzaei, T. M. Monro, Y. S. Kivshar, and S. Afshar V., "Strong magnetic response of optical nanofibers," *ACS Photon.*, vol. 3, no. 6, pp. 972–978, Jun. 2016.

[29] J. M. M. Hall, T. Reynolds, M. R. Henderson, N. Riesen, T. M. Monro, and S. Afshar, "Unified theory of whispering gallery multilayer microspheres with single dipole or active layer sources," *Opt. Exp.*, vol. 25, no. 6, p. 6192, 2017.

[30] Y. Qin, Y. Fang, L. Wang, S. Tang, S. Sun, Z. Liu, and Y. Mei, "Surface wave resonance and chirality in a tubular cavity with metasurface design," *Opt. Commun.*, vol. 417, pp. 42–45, Jun. 2018.

[31] P. Moitra, B. A. Slovick, W. Li, I. I. Kravchencko, D. P. Briggs, S. Krishnamurthy, and J. Valentine, "Large-scale all-dielectric metamaterial perfect reflectors," *ACS Photon.*, vol. 2, no. 6, pp. 692–698, Jun. 2015.

[32] A. Monti, A. Alu, A. Toscano, and F. Bilotti, "Surface impedance modeling of all-dielectric metasurfaces," *IEEE Trans. Antennas Propag.*, vol. 68, no. 3, pp. 1799–1811, Mar. 2020.

[33] D. Lin, M. Melli, E. Poliakov, P. S. Hilaire, S. Dhuey, C. Peroz, S. Cabrini, M. Brongersma, and M. Klug, "Optical metasurfaces for high angle steering at visible wavelengths," *Sci. Rep.*, vol. 7, no. 1, Dec. 2017, Art. no. 2286.

[34] D. Headland, S. Nirantar, W. Withayachumnankul, P. Gutruf, D. Abbott, M. Bhaskaran, C. Fumeaux, and S. Sriram, "Terahertz magnetic mirror realized with dielectric resonator antennas," *Adv. Mater.*, vol. 27, no. 44, pp. 7137–7144, Nov. 2015.

[35] X. Liu, I. V. Shadrivov, K. Fan, and W. J. Padilla, "Experimental realization of a terahertz all-dielectric metasurface absorber," *Opt. Exp.*, vol. 25, no. 1, pp. 191–201, Jan. 2017.

[36] D.-H. Kwon, G. Ptitcyn, A. Díaz-Rubio, and S. A. Tretyakov, "Transmission magnitude and phase control for polarization-preserving reflectionless metasurfaces," *Phys. Rev. A, Gen. Phys.*, vol. 9, no. 3, Mar. 2018, Art. no. 034005.

[37] A. Wu, H. Li, J. Du, X. Ni, Z. Ye, Y. Wang, Z. Sheng, S. Zou, F. Gan, X. Zhang, and X. Wang, "Experimental demonstration of in-plane negative-angle refraction with an array of silicon nanoposts," *Nano Lett.*, vol. 15, no. 3, pp. 2055–2060, Mar. 2015.

[38] Q. Yang, S. Kruk, Y. Xu, Q. Wang, Y. K. Srivastava, K. Koshelev, I. Kravchenko, R. Singh, J. Han, Y. Kivshar, and I. Shadrivov, "Mie-resonant membrane huygens' metasurfaces," *Adv. Funct. Mater.*, vol. 30, no. 4, 2020, Art. no. 1906851.

[39] A. K. González-Alcalde, M. A. G. Mandujano, R. Salas-Montiel, L. O. Le Cunff, G. Lerondel, and E. R. Méndez, "Magnetic mirror metasurface based on the in-phase excitation of magnetic dipole and electric quadrupole resonances," *J. Appl. Phys.*, vol. 125, no. 24, Jun. 2019, Art. no. 243103.

[40] J. Tian, H. Luo, Q. Li, X. Pei, K. Du, and M. Qiu, "Near-infrared super-absorbing all-dielectric metasurface based on single-layer germanium nanostructures," *Laser Photon. Rev.*, vol. 12, no. 9, Sep. 2018, Art. no. 1800076.

[41] R. Paniagua-Domínguez, Y. F. Yu, A. E. Miroshnichenko, L. A. Krivitsky, Y. H. Fu, V. Valuckas, L. Gonzaga, Y. T. Toh, A. Y. S. Kay, B. Luk'yanchuk, and I. Arseniy Kuznetsov, "Generalized brewster effect in dielectric metasurfaces," *Nature Commun.*, vol. 7, no. 1, 2016, Art. no. 10362.

[42] I. Al-Naib and W. Withayachumnankul, "Recent progress in terahertz metasurfaces," *J. Infr., Millim., THz Waves*, vol. 38, no. 9, pp. 1067–1084, Sep. 2017.

[43] J. He, T. Dong, B. Chi, and Y. Zhang, "Metasurfaces for terahertz wavefront modulation: A review," *J. Infr., Millim., THz Waves*, vol. 5, pp. 1–25, Feb. 2020.

[44] H. Song, L. Sun, and G. P. Wang, "Tunable perfect magnetic mirrors and retroreflectors in terahertz band," *Opt. Exp.*, vol. 28, no. 1, pp. 753–759, 2020.

[45] D. Wang, L. Zhang, Y. Gong, L. Jian, T. Venkatesan, C.-W. Qiu, and M. Hong, "Multiband switchable terahertz quarter-wave plates via phase-change metasurfaces," *IEEE Photon. J.*, vol. 8, no. 1, Feb. 2016, Art. no. 5500308.

[46] L. Cong, N. Xu, J. Gu, R. Singh, J. Han, and W. Zhang, "Highly flexible broadband terahertz metamaterial quarter-wave plate," *Laser Photon. Rev.*, vol. 8, no. 4, pp. 626–632, Jul. 2014.

[47] W. S. Lee, R. T. Ako, M. X. Low, M. Bhaskaran, S. Sriram, C. Fumeaux, and W. Withayachumnankul, "Dielectric-resonator metasurfaces for broadband terahertz quarter-and half-wave mirrors," *Opt. Exp.*, vol. 26, no. 11, pp. 14392–14406, 2018.

[48] S. Atakaramians, I. V. Shadrivov, A. E. Miroshnichenko, A. Stefani, H. Ebendorff-Heidepriem, T. M. Monro, and S. Afshar V., "Enhanced terahertz magnetic dipole response by subwavelength fiber," *APL Photon.*, vol. 3, no. 5, May 2018, Art. no. 051701.

[49] V. O. Byelobrov, T. L. Zinenko, K. Kobayashi, and A. I. Nosich, "Periodicity matters: Grating or lattice resonances in the scattering by sparse arrays of subwavelength strips and wires.," *IEEE Antennas Propag. Mag.*, vol. 57, no. 6, pp. 34–45, Dec. 2015.

[50] M. Chen, F. Fan, S.-T. Xu, and S.-J. Chang, "Artificial high birefringence in all-dielectric gradient grating for broadband terahertz waves," *Sci. Rep.*, vol. 6, no. 1, Dec. 2016, Art. no. 38562.

[51] S. I. Maslovski, S. A. Tretyakov, and P. A. Belov, "Wire media with negative effective permittivity: A quasi-static model," *Microw. Opt. Technol. Lett.*, vol. 35, no. 1, pp. 47–51, Oct. 2002.

[52] S. I. Maslovski and M. G. Silveirinha, "Nonlocal permittivity from a quasistatic model for a class of wire media," *Phys. Rev. B, Condens. Matter*, vol. 80, no. 24, Dec. 2009, Art. no. 245101.

[53] S. Atakaramians, S. Afshar Vahid, B. M. Fischer, H. Ebendorff-Heidepriem, T. Monro, and D. Abbott, "Microwire fibers for low-loss THz transmission," in *Proc. Smart Struct., Devices, Syst.*, Dec. 2006, p. 64140.

[54] M. Naftaly and R. E. Miles, "A method for removing etalon oscillations from THz time-domain spectra," *Opt. Commun.*, vol. 280, no. 2, pp. 291–295, Dec. 2007.

[55] Y. Cao, K. Nallappan, H. Guerboukha, T. Gervais, and M. Skorobogatiy, "Additive manufacturing of resonant fluidic sensors based on photonic bandgap waveguides for terahertz applications," *Opt. Exp.*, vol. 27, no. 20, pp. 27663–27681, 2019.

[56] W. Liu, "Generalized magnetic mirrors," *Phys. Rev. Lett.*, vol. 119, no. 12, Sep. 2017, Art. no. 123902.

[57] J. Dai, J. Zhang, W. Zhang, and D. Grischkowsky, "Terahertz time-domain spectroscopy characterization of the far-infrared absorption and index of refraction of high-resistivity, float-zone silicon," *J. Opt. Soc. Amer. B, Opt. Phys.*, vol. 21, no. 7, pp. 1379–1386, 2004.

QIGEJIAN WANG (Graduate Student Member, IEEE) received the B.S. degree in optoelectronic information science and engineering from the Huazhong University of Science and Technology (HUST), Wuhan, China, in 2017. He is currently pursuing the M.Phil. degree with the School of Electrical Engineering and Telecommunications, University of New South Wales (UNSW), Sydney, Australia.

From 2016 to 2017, he was a Thesis Student with the Wuhan National Laboratory for Optoelectronics, Wuhan, China. His research interests include terahertz photonics and metasurface. He is also a Student Member of OSA and SPIE.

SHAHRAAM AFSHAR V. received the Ph.D. degree in physics, laser, and nonlinear optics from The University of Adelaide, in 2001. In 2001, he held a postdoctoral position the Fibre Optics Group, University of Ottawa, where he worked on fibre-optic, distributed, strain, and temperature sensors based on Brillouin scattering. In 2005, he joined the Centre of Expertise in Photonics (CoEP), The University of Adelaide, which later formed into the Institute for Photonics and Advanced Sensing (IPAS). In 2015, he was a member of a team to form Laser Physics and Photonic Devices Laboratories, School of Engineering, University of South Australia. He is currently an Associate Professor with Laser Physics and Photonic Devices Laboratories, University of South Australia, STEM. He has been active in the field of nonlinear processes in subwavelength waveguides and radiation of dipoles in vicinity of optical fibres. As a new activity and more than the last couple of years, his team has been working on nonlinear Fourier transform for high capacity fibre optic communication. His research interests include optical processes in high index waveguides with complex structures and their applications for linear and nonlinear processes.

HEIKE EBENDORFF-HEIDEPRIEM received the Ph.D. degree in chemistry from the University of Jena, Germany, in 1994. From 2001 to 2004, she was with the Optoelectronics Research Centre, University of Southampton, U.K. Since 2005, she has been with The University of Adelaide, Australia. She currently leads the Fibers and Photonics Materials Research Group and also the Deputy Director of the Institute for Photonics and Advanced Sensing. She is also the Deputy Director of the Optofab Node of the Australian National Fabrication Facility (ANFF) and Senior Investigator of the ARC Centre of Excellence for Nanoscale BioPhotonics (CNBP). Her research interests include the development of novel optical glasses, specialty optical fibers, hybrid glasses and fibers, surface functionalization and sensing approaches. She received the Weyl International Glass Science Award and the prestigious Marie Curie Individual Fellowship of the European Union, in 2001.

SHAGHIK ATAKARAMIANS (Senior Member, IEEE) received the B.S. degree in telecommunication engineering from the Iran University of Science and Technology (IUST), the M.S. degree in telecommunication engineering from the University of Tehran, and the Ph.D. degree in electrical & electronic engineering from The University of Adelaide, Australia, in 2011, with a Certificate of Merit from the Dean. Her Ph.D. thesis received the Gertrude Rohan Memorial Prize and the 2011 University Doctoral Research Medal for outstanding research.

She was with the Institute of Photonics and Optical Science (IPOS), from 2011 to 2017, and also with the Centre for Ultrahigh bandwidth Devices for Optical Systems (CUDOS), from 2012 to 2014, with the University of Sydney first as a Postdoctoral Fellow and then as a Research Fellow. She is currently a Scientia Senior Lecturer and a Team Lead of the THz Photonics Lab, School of Electrical Engineering and Telecommunications, UNSW, Sydney. Her research interests include terahertz waveguides, meta-waveguides, and meta-devices. She is a Senior OSA Member. She was awarded the Australian Research Council (ARC) Discovery Early Career Researcher Award (DECRA), in 2014. She is an Associate Editor of the *APL Photonics*, AIP publishing.